ACS APPLIED MATERIALS & INTERFACES

www.acsami.org

Research Article

Computational Design to Suppress Thermal Runaway of Li-Ion Batteries via Atomic Substitutions to Cathode Materials

Yuki Yoshimoto,* Takahiro Toma, Kenta Hongo, Kousuke Nakano, and Ryo Maezono

Cite This: *ACS Appl. Mater. Interfaces* 2022, 14, 23355−23363

Read Online

ACCESS | Metrics & More | Article Recommendations | Supporting Information

ABSTRACT: The cathode material of a lithium-ion battery is a key component that affects durability, capacity, and safety. Compared to the $LiCoO_2$ cathode material (the reference standard for these properties), $LiNiO_2$ can extract more Li at the same voltage and has therefore attracted considerable attention as a material that can be used to obtain higher capacity. As a trade-off, it undergoes pyrolysis relatively easily, leading to ignition and explosion hazards, which is a challenge associated with the application of this compound. Pyrolysis has been identified as a structural phase transformation of the layered rocksalt structure → spinel → cubic rocksalt. Partial substitution of Ni with various elements can reportedly suppress the transformation and, hence, the pyrolysis. It remains unclear which elemental substitutions inhibit pyrolysis and by what mechanism, leading to costly material development that relies on empirical trial and error. In this study, we developed several possible reaction models based on existing reports, estimated the enthalpy change associated with the reaction by ab initio calculations, and identified promising elemental substitutions. The possible models were narrowed down by analyzing the correlations of the predicted dependence of the reaction enthalpies on elemental substitutions, compared between different reaction models. According to this model, substitution by P and Ta affords the highest enthalpy barrier between the initial (layered rocksalt) and the final (cubic rocksalt) structures but promotes the initial transformation to spinel as a degradation. Substitution by W instead generates the barrier to the final (preventing dangerous incidents) process, as well as for the initial degradation to spinel; therefore, it is a promising strategy to suppress the predicted pyrolysis.

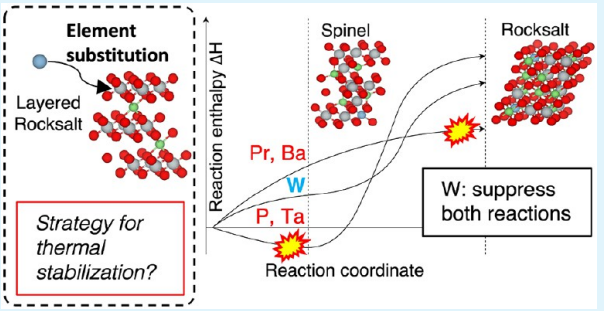

KEYWORDS: *ab initio calculation, lithium-ion battery, cathode materials, thermal runaway, atomic substitution*

1. INTRODUCTION

Lithium-ion batteries (LIBs) have become an indispensable technology to achieve carbon neutrality: they offer longer operational time for electronic devices, longer cruising distance for electric vehicles, clean power storage, etc. The cathode material is one of the primary LIB components that affects durability, capacity, safety, and price. There have been cumulative efforts to improve its operating characteristics since the LIB was first commercialized.[1−11] In particular, $LiNiO_2$-based cathode materials (LNOs) have been investigated thoroughly because of their cost effectiveness as well as the potentially better battery capacity compared to $LiCoO_2$ (LCO).[11] For the same voltage, LNO can provide more Li ions than LCO, leading to the higher battery capacity. Though LNO has found applications in commercial products, thermal instability in the charged state has been recognized as a problem to be addressed. Higher amounts of Li being extracted in the charged state result in a reduced lattice structural stability, which leads to thermal instability.[12] When LNO in the charged state is subjected to high temperatures, a pyrolysis reaction occurs, causing a phase transition with desorbing oxygen gas.[14,16,17] Desorbed oxygen gas reacts with the electrolyte to produce carbon dioxide gas while generating intense heat.[13−15] Battery cells eventually undergo thermal runaway, presenting the danger of ignition and explosion. Therefore, to ensure safety, it is necessary to improve thermal stability against pyrolysis.

According to previous experiments, the thermal decomposition of LNO at the charged-up state is understood to be a reaction process from a layered rocksalt structure to a spinel structure and, finally, to a cubic rocksalt structure, with a combination of cation mixing and oxygen desorption.[16−19] Suppression of any of these phase transitions is considered to be efficient against the thermal decomposition. A number of studies have revealed that atomic substitutions could suppress the phase transition to improve the thermal instability. Atomic substitutions by B,[20] Na,[21] Mg,[22] Al,[23] K,[24] Ti,[25] Ga,[26] Rb,[27]

Received: January 26, 2022
Accepted: May 4, 2022
Published: May 16, 2022

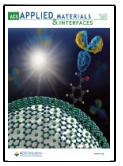

Y,[28] and Zr[29] are reported to be efficient in suppressing any of the structural transitions, leading to improved mechanical properties and structural stability. The substitutions by Ti,[30] Y,[28] Zr,[31] Sb,[32] and W[33] are reported to suppress the amount of desorbed oxygen, via which the structural transition is suppressed, resulting in structural stability of the charged-up state. The stability was also analyzed using ab initio calculations in a previous study,[34] but there have been no analyses on the atomic substitution effect so far.

Though knowledge to improve the thermal stability of LNO by atomic substitutions is growing, it remains limited within each individual element, not comprehensive over the elemental trend. The current design for thermal stability still relies on empirical trial and error of multiple species to be doped, referring to each of these individual pieces of knowledge, costing much in synthesis to find the best combination of elements. It would be desirable to analyze and understand the mechanism of each substituent element and have a comprehensive view for the design.

To overcome this difficulty, we conducted an analysis to quantify and compare the improvement in thermal stability by elemental substitution by constructing several possible reaction model candidates based on existing reports.[16−19]

With comparisons of differential scanning calorimetry (DSC) experiments, we narrowed down the candidates for the reaction models. For the narrowed down possibilities, we estimated and compared the reaction enthalpies to estimate which elemental substitution is effective to suppress the reaction for thermal decomposition. The thermal decomposition process was analyzed by separating the initial conversion to the spinel and final transformation to the rocksalt. Each could correspond to the suppression against degradation and the safety against thermal runaway. We provided a computational prediction of elemental substitution that would be desirable to deter each factor.

2. REACTION MODELS

Taking the pristine layered rocksalt structure, $LiNiO_2$ = $Li_{12}Ni_{12}O_{24}$, its charged-up composition of the high-capacity cathode material is modeled as $Li_2Ni_{12}O_{24}$ (corresponding to a composition of 83.3% of Li extracted).

The substituting element M was assumed to replace one of the 12 Ni sites, resulting in a solid solution $Li_2Ni_{11}MO_{24}$ (substituting concentration is 8.3%). We considered 60 potential candidates for the substituting element M: the elements from Mg to Bi, excluding groups 1, 16, 17, and 18. For the resultant layered rocksalt structure $Li_2Ni_{11}MO_{24}$, we considered the pyrolysis reactions to the spinel and cubic rocksalt structure (Figure 1 illustrates example structures).[16−19]

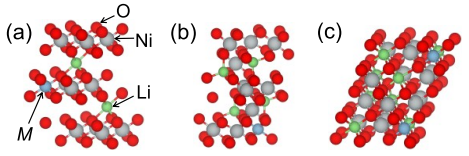

Figure 1. Example structures considered in reaction models: (a) layered rocksalt structure $Li_2Ni_{11}MO_{24}$, (b) spinel structure $Li_6Ni_{11}MO_{24}$, and (c) (cubic) rocksalt structure $Li_{12}Ni_{11}MO_{24}$, where M indicates a substituting element (see text). Structures were drawn by VESTA.[35]

In the conventional low-capacity cathode material, the sequence [layered rocksalt] → [spinel] → [rocksalt] is clearly observed.[19] In contrast, high-capacity materials with a Ni content of approximately 80% exhibit pyrolysis, quickly decomposing via a two-phase segregation composed of spinel and cubic rocksalt. In situ XRD experiments have reported that the spinel single phase is maintained only in a very narrow temperature range ($\Delta T \sim 10$ °C).[19] Accordingly, we considered several candidate models for the reaction, including the possibility of the path without spinel as metastable. These multiple candidates were narrowed down according to the method as described in Section 3.

We denote by $Li_lNi_nM_mO_k$ the composition of the spinel and rocksalt structures. The ratios of cations to the anion, $(l + n + m):k$, for spinel and cubic rocksalt, are 3:4 and 1:1, respectively. For the initial conversion, [Initial] → [Intermediate(Spinel)], we considered two models: [(1; Spinel/Free), (2; Spinel/Restricted)]. For the whole transition, [Initial] → [Final (Rocksalt)], we considered three possibilities: [(3; Rocksalt/Free), (4; Rocksalt/Suppressed), (5; Rocksalt/Restricted)].

The labels "Free", "Suppressed", and "Restricted" represent the difference with respect to the change in the ratio l:n (Li:Ni) by the reaction (termed as Li-partitioning).

"Free" models allow Li-partitioning[34] whereas "Restricted" models do not.[16−19] "Suppressed" corresponds to models with lower Li-partitioning. Since the pyrolysis of $LiNiO_2$ occurs at a relatively lower temperature, less than 250 °C,[16,17] we did not consider the possibility of partitioning for other elements; that is, we assume that the ratio n:m is fixed.

2.1. Spinel/Free. For the initial conversion, [Initial] → [Intermediate(Spinel)], it was reported in a theoretical study[34] that the following process would be the stable path, allowing Li-partitioning:

$$Li_2Ni_{11}MO_{24} \rightarrow \frac{1}{3}Li_6Ni_{11}MO_{24} + \frac{2}{3}Ni_{11}MO_{16} + \frac{8}{3}O_2\uparrow \quad (1)$$

The first and second terms on the right-hand side are spinel structures with $(l + n + m):k$ = 3:4. Owing to Li-partitioning, the first term gains more Li while the second term loses it, forming a two-phase segregation. The third term denotes the desorbed oxygen.

2.2. Spinel/Restricted. Several studies on the initial conversion, [Initial] → [Intermediate(Spinel)], propose the possibility that the reaction occurs prohibiting Li-partitioning.[16−19] The process is modeled as

$$Li_2Ni_{11}MO_{24} \rightarrow Li_2Ni_9MO_{16} + \frac{1}{6}Ni_{11}MO_{16} + \frac{8}{3}O_2\uparrow \quad (2)$$

This model is an approximation that allows us to handle the ab initio simulation with a tractable cost: the prohibition of Li-partitioning leads to a fixed ratio of n:m = 11:1 (as in the left-hand side and in the second term on the right-hand side); however, the ratio n:m in the first term on the right-hand side is 9:1, which we approximate as 11:1. Without such an approximation, the requisite simulation cell gets too large and makes the analysis intractable.

2.3. Rocksalt/Free. For the [Initial] → [Final (Rocksalt)], a reaction model allowing the Li-partitioning is represented as

https://doi.org/10.1021/acsami.2c01607
ACS Appl. Mater. Interfaces 2022, 14, 23355−23363

$$Li_2Ni_{11}MO_{24} \rightarrow \frac{1}{6}Li_{12}Ni_{11}MO_{24} + \frac{5}{6}Ni_{11}MO_{12} + 5O_2\uparrow \quad (3)$$

where both the first and the second terms on the right-hand side satisfy $(l + n + m):k = 1:1$, the cubic rocksalt structure.

Owing to the partitioning, the first term gains more Li while the second term loses it, forming a two-phase segregation.

2.4. Rocksalt/Suppressed. Another reaction model for the [Initial] → [Final (Rocksalt)], with Li-partitioning more suppressed than in eq 3, is given as

$$Li_2Ni_{11}MO_{24} \rightarrow \frac{1}{3}Li_6Ni_{11}MO_{18} + \frac{2}{3}Ni_{11}MO_{12} + 5O_2\uparrow \quad (4)$$

where both the first and the second terms on the right-hand side realize $(l + n + m):k = 1:1$, the cubic rocksalt structure.

The first term represents the phase with increased Li, but its concentration is lower than that of the first term in eq 3.

2.5. Rocksalt/Restricted. As a model for [Initial] → [Final (Rocksalt)] with Li-partitioning prohibited, we adopt

$$Li_2Ni_{11}MO_{24} \rightarrow Li_2Ni_{11}MO_{14} + 5O_2\uparrow \quad (5)$$

3. METHOD

For the candidates proposed above, we narrowed down the possibility by comparing with experiments as explained below. We excluded the "Restricted" processes (eqs 2 and 5) from the candidates.

We refer to the experimentally observed variation in T_{DSC} dependent on the substituent M. Here, T_{DSC} denotes the temperature at a peak of the DSC curve (experimental details are given in the SI). Usually, T_{DSC} corresponds to the temperature at which the pyrolysis reaction occurs. The temperature, hence, scales with the difference

$$T_{DSC} \sim \Delta H/\Delta S \quad (6)$$

where ΔH and ΔS, respectively, denote the change in enthalpy and entropy before and after the reaction, as included in the change in Gibbs energy. The dependence $T_{DSC}(M)$ with respect to the substituents M is shown and listed in Figure 2 and Table 1, respectively. When we limit M to a mere 8% substitution, it is reasonable to assume that the reaction path is independent of M. In this case, ΔS would primarily be due to the contribution of oxygen gas.[34] This is expected to have negligible M-dependence, leading to

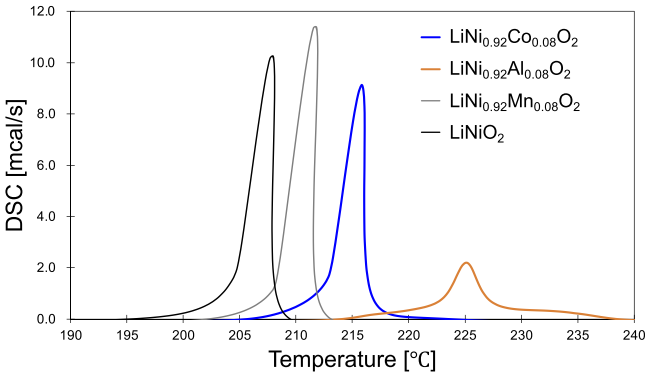

Figure 2. Temperature dependence of differential scanning calorimetry (DSC) curves. The temperature at a peak of the DSC curve, T_{DSC}, corresponds approximately to the pyrolysis temperature.

Table 1. Dependence of T_{DSC} on the Substituent M as Given in Figure 2

substituent M	T_{DSC}
Ni	207.99
Mn	211.83
Co	215.82
Al	225.07

$$T_{DSC}(M) \propto \Delta H(M) \quad (7)$$

Assuming that the solid phases on the right-hand side of each reaction model are all at phase segregation, we can estimate $\Delta H(M)$ as the energy difference between the crystals appearing on the left- and the right-hand side, which can be computed by ab initio calculations. In this manner, we expect that the trend of $T_{DSC}(M)$ can be explained by $\Delta H(M)$ using ab initio calculations. With α denoting the index for each reaction model (Spinel/Free, Spinel/Restricted, ...), we evaluate $\Delta H^{(\alpha)}(M)$ for each α. Then, from the set of candidates, we eliminate α models that do not satisfactorily explain the observed dependence $T_{DSC}(M)$. Each ab initio calculation to compute $\Delta H(M)$ involves tedious procedures to obtain plausible structure models after the combinations of geometrical optimizations applied to the lattice with atomic substitutions under the consideration of spatial symmetric operations. This process is detailed in the SI.

Figure 3 shows the correlation between $T_{DSC}(M)$ and $\Delta H^{(\alpha)}(M)$. Each line corresponds to a reaction model indexed

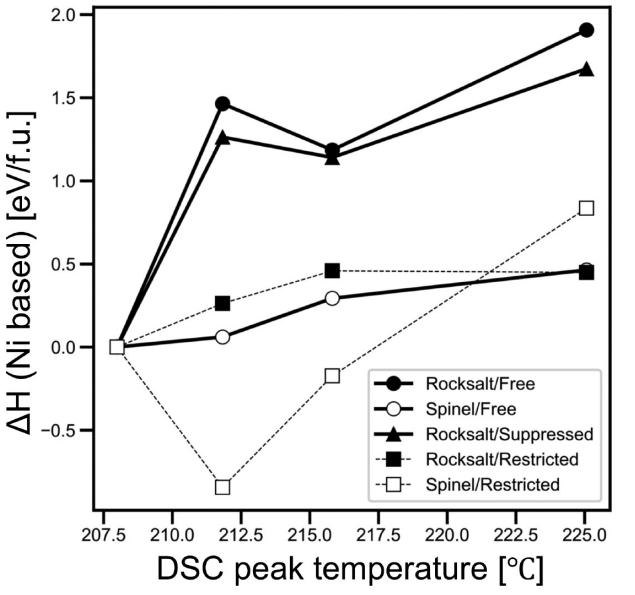

Figure 3. Correlation between $T_{DSC}(M)$ and $\Delta H^{(\alpha)}(M)$ evaluated for reaction models, eqs 1–5. $\Delta H^{(\alpha)}(Ni)$ is taken as the zero reference. The four plot points in each line correspond to the choice of substituents M (= Ni, Mn, Co, Al) as given in Figure 2 and Table 1. Open (filled) symbols mean spinel (rocksalt) structure. Circle, rectangular, and triangle symbols correspond to "Free", "Restricted", and "Suppressed", respectively.

as α, and the four plotted points correspond to the choice of substituents M (= Ni, Mn, Co, Al) as given in Figure 2 and Table 1. The plot shows that the model α = "Spinel/Restricted" exhibits a poor correlation, which justifies its rejection as a candidate. As per the literature that discusses

https://doi.org/10.1021/acsami.2c01607
ACS Appl. Mater. Interfaces 2022, 14, 23355−23363

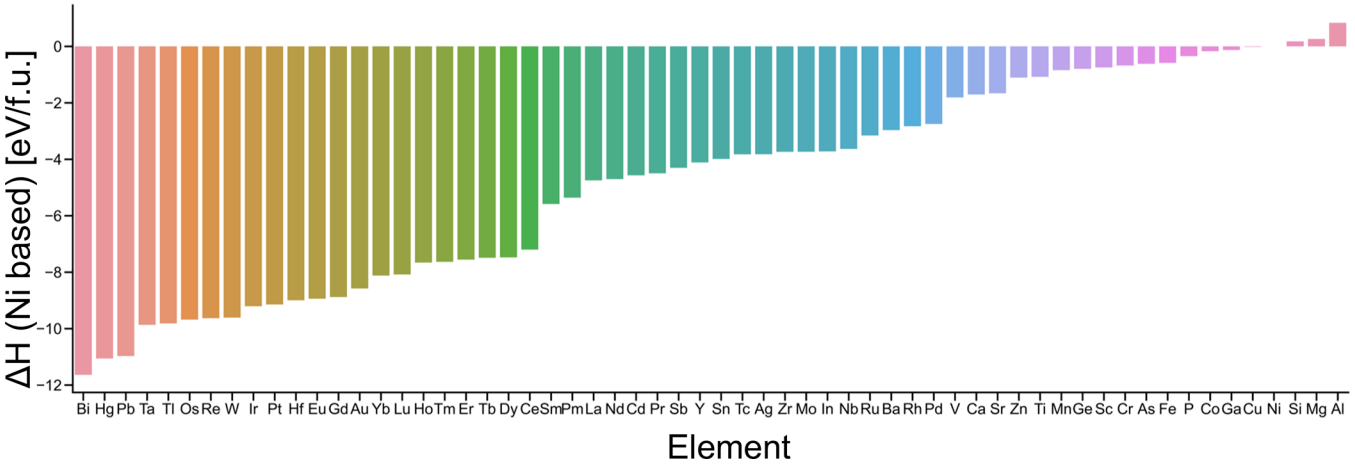

Figure 4. Enthalpy change evaluated for the reaction model eq 2 (Spinel/Restricted), $\Delta H^{(\text{Spinel/Restricted})}(\text{M})$. Because the reference zero for the vertical axis is taken to be $\Delta H^{(\text{Spinel/Restricted})}(\text{Ni})$, the negative predictions, except for M = Si, Mg, and Al, mean that the pyrolysis temperature decreases (i.e., becomes worse against pyrolysis), which contradicts experimental reports.

phase stability using first-principles calculations, the Li-diluted spinel phase ($Li_3Ni_{12}O_{20}$) is not an equilibrium phase.[34] This result indicates that a monotectoid reaction occurs under a quasistatic process. Therefore, this contradiction between the present experimental results and the Spinel/Restricted model is because the Li-partitioning is sufficient in reality and quickly forms the equilibrium phase, such as the ($LiNi_2O_4$) spinel phase.

Furthermore, the predictions of the model α = "Spinel/Restricted" contradict experimental observations. Figure 4 shows the dependence, $\Delta H^{(\text{Spinel/Restricted})}(\text{M})$. Because the reference zero for the vertical axis is taken to be $\Delta H^{(\text{Spinel/Restricted})}(\text{Ni})$, the negative predictions—except for M = Si, Mg, and Al—mean that the pyrolysis temperature is lowered (i.e., becomes worse against pyrolysis). This contradicts experimental observations[20−33] that report that the substituents improve the property against pyrolysis.

4. RESULTS AND DISCUSSION

4.1. Choosing a Model for Predictions. According to the analyses presented using Figures 3 and 4, we eliminate the "Spinel/Restricted" model from the set of candidates. Among the rest, "Spinel/Free" promotes Li-partitioning, and the consequent reaction toward the rocksalt structure should also promote partitioning. Therefore, we exclude "Rocksalt/Restricted", prohibiting the Li-partitioning.

Of the remaining possibilities corresponding to the rocksalt structure, "Rocksalt/Free" (eq 3) and "Rocksalt/Suppressed" (eq 4), it does not matter which model we adopt as long as we focus on the M-substitution effect. We explain this in the following discussion (Figure 5).

We consider the M-substitution dependence of the pyrolysis enthalpy change $\Delta H(\text{M})$ for two different reaction models and analyze the correlation between the predicted values. Figures 5 and 6 show the corresponding correlation plots. If considerable correlations are obtained, then it can be said that the prediction does not depend on the adopted model. Figure 5 compares the models "Rocksalt/Free"(eq 3) and "Rocksalt/Suppressed"(eq 4) which show fairly high correlation, indicating that the prediction of the M-substitution effect is identical regardless of the adopted model. Therefore, as long as we discuss the M-substitution effect, we can narrow down the

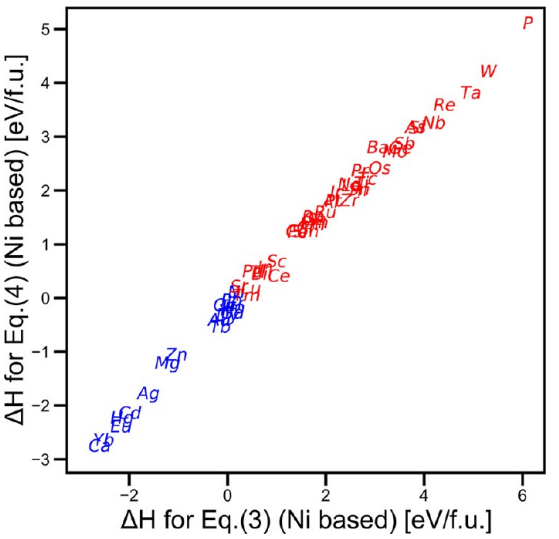

Figure 5. Correlation between the M-substitution dependence of the pyrolysis enthalpy change $\Delta H(\text{M})$ predicted by two different reaction models. Plotting points are shown by the name of elements wherein blue (red) indicates that the element enhances (depresses) the pyrolysis. The plot compares "Rocksalt/Free" (eq 3) and "Rocksalt/Suppressed" (eq 4) models. The plot shows a fairly high correlation, implying that the prediction of the M-substitution effect is identical regardless of the adopted model.

model possibility as "Layered Rocksalt" → "Spinel/Free" (eq 1) → "Rocksalt/Free" (eq 3).

Once a reaction path to be considered is fixed as above ("Free" model that allows Li-partitioning), the next question concerns the enthalpy change. To capture the substitution effect of M, should we adopt the enthalpy change of (a) the most initial reaction process (to Spinel, eq 1) or that of (b) the whole reaction process (to Rocksalt, eq 3)? Figure 6 shows the correlation between the predictions of each model. The correlation is weak, indicating that the prediction of the M-substitution effect depends on the adopted model. The elements that deviate significantly from the linear fitting (dashed line) in the figure (P deviating to the left and Pr deviating to the right) correspond to such M whose prediction varies greatly depending on the model choice. Group a (eq 1),

https://doi.org/10.1021/acsami.2c01607
ACS Appl. Mater. Interfaces 2022, 14, 23355−23363

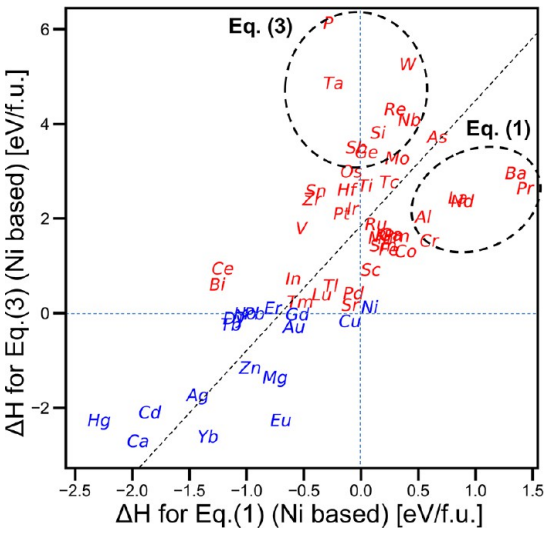

Figure 6. Correlation of the M-substitution dependence of the pyrolysis enthalpy change $\Delta H(M)$ predicted by two different reaction models. Plotting points are shown by the name of elements wherein blue (red) indicates that the element enhances (depresses) the pyrolysis. Fixing a reaction path to be considered as a "Free" model which allows Li-partitioning, the plot considers the correlation between the predictions based on the initial reaction process (to Spinel, eq 1, horizontal) and the whole process (finally to Rocksalt, eq 3, vertical).

headed by M = Pr, is the type that greatly suppresses the initial reaction (→Spinel), but once it is cleared, reaching the final stage (→Rocksalt) is relatively easy. In contrast, the group headed by M = P (group b) is of the type that easily clears the initial reaction (→ Spinel) but is well-suppressed in arriving to the final (→Rocksalt), as schematically depicted in Figure 7.

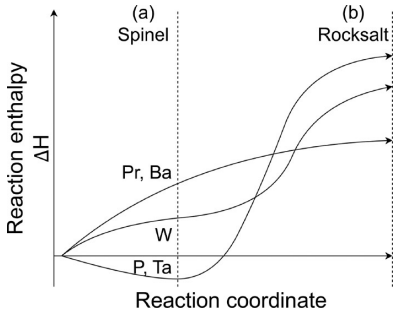

Figure 7. Schematic representation of the results obtained in Figure 6. The suppression of the pyrolysis can be decomposed into that against the initial reaction (a) and that against the final transition (b). The diagram is just a schematic, with no specific meaning ascribed to the curvatures of the paths.

Next, we comment on the correspondence between the results presented in Figure 6 and the experimental results in the literature. Most of the effective elements presented in the Introduction are predicted to be elements that inhibit the transformation to the spinel or rocksalt, which is the qualitative trend of the effect of elemental substitution that has been reproduced.[23,25−27,29−33] However, it was observed that elements such as Mg[22] and Y,[28] which were reported to stabilize the layered rocksalt, did not inhibit pyrolysis. The feature of these elements is that they do not have factors that reduce the stability of the post-transformation phases, such as high valence or expansion of ionic radius. This suggests that the evaluation of thermal stability should consider the post-transformation phases and not only the stability of the layered rocksalt.

4.2. Causes of the Difference in Predicted Trends. As shown in Figure 7, different models (a and b) predict different order for the preferred substituents. While the analysis using the whole reaction model (eq 3) prefers M = P and Ta, they are predicted to promote starting the initial reaction (eq 1) which is a negative property. To suppress the onset of the initial reaction, the choice M = Pr and Ba is preferred, but they are worse in suppressing the final process compared to M = P, Ta, and W. From the fundamentals of reaction theory, one might think that it is sufficient to focus on the suppression of the most initial reaction, eq 3, thereby eliminating M = P and Ta as a bad choice. However, as explained in the first paragraph in Section 2, the present targets (high-capacity materials with Ni content around 80%) exhibit such behavior not like a clear reaction order as "Spinel → Rocksalt". As such, we do not want to exclude M = P and Ta immediately, and we retain them as candidates for suppressing pyrolysis.

Let us investigate the factor that brings about the difference of the preferred M between eqs 1 and 3. Comparing the two processes, we notice that the difference includes two factors, namely, (i) different structures (spinel and rocksalt) and (ii) different amounts of desorbed oxygen (5 or 8/3 of O_2). To identify the factor that matters, we need a reference which differs in only one factor while keeping the other factor unchanged. With such a reference, we can prepare a model keeping the same amount of the desorbed oxygen ($5O_2$) as in eq 3 but with a different structure (spinel) as

$$Li_2Ni_{11}MO_{24} \rightarrow \frac{1}{3}Li_6Ni_{11}MO_{18}V_{O6} + \frac{2}{3}Ni_{11}MO_{12}V_{O4} + 5O_2\uparrow \quad (8)$$

where V_O indicates an oxygen vacancy. The reference reaction toward spinel (compared to other models as shown in Figure 8) is accompanied by the vacancy sites emitting further oxygen

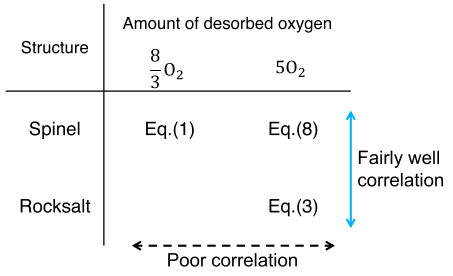

Figure 8. Comparisons among different reaction models including the reference eq 8. The figure summarizes the results of Figures 9 and 10, namely, the poor (good) correlation for the difference in the amount of desorbed oxygen (in the structures).

to achieve increased desorption the same as that toward Rocksalt (eq 3; details of the structure, including oxygen defect positions, are shown in the SI). This model is a hypothetical model constructed to discuss the difference between the Rocksalt/Free and Spinel/Free models in terms of their predictive tendencies. As a result, the model is not based on experimental results and may be energetically unstable.

By using the reference (eq 8), we can examine the correlations (i) between eqs 8 and 3 for the structure

https://doi.org/10.1021/acsami.2c01607
ACS Appl. Mater. Interfaces 2022, 14, 23355−23363

difference (Figure 9) and (ii) between eqs 8 and 1 for the difference in the amount of desorbed oxygen (Figure 10).

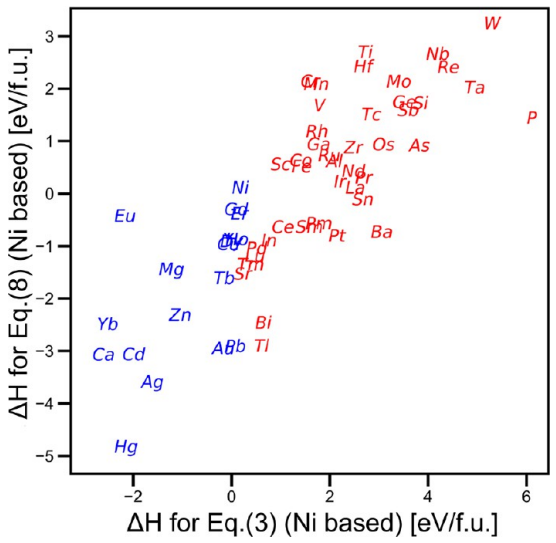

Figure 9. Correlation between the M-substitution dependence of the pyrolysis enthalpy change, ΔH(M), predicted by two different reaction models. Plotted points are shown by the name of elements wherein blue (red) indicates that the element enhances (depresses) the pyrolysis. The correlation with the reference model eq 8 indicates how the difference in the crystal structure affects the prediction of preferred substituent M (worse, it matters more), as the two models have the same amount of desorbed oxygen (see Figure 8).

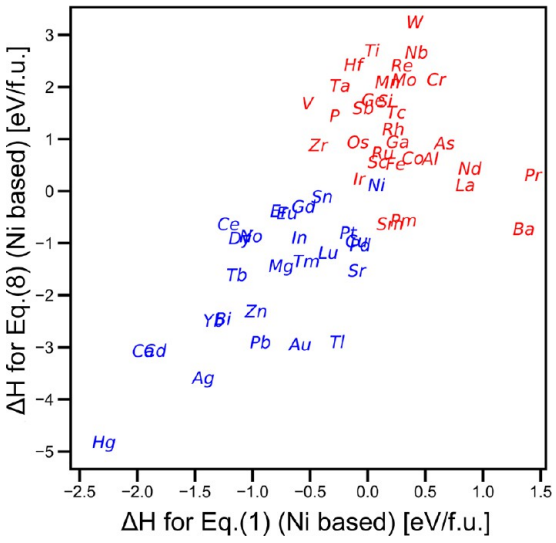

Figure 10. Correlation between the M-substitution dependence of the pyrolysis enthalpy change ΔH(M) predicted by two different reaction models. Plotted points are shown by the name of elements wherein blue (red) indicates that the element enhances (depresses) the pyrolysis. The correlation with the reference model eq 8 indicates how the difference of the amount of desorbed oxygen matters in the prediction of preferred substituent M (worse, it matters more), because two models have the same crystal structure (see Figure 8).

Comparing the results in Figures 9 and 10, we observe that Figure 10 gives a worse correlation, implying that the different amount of desorbed oxygen matters more in the prediction of the preferred choice of M. We can then speculate that the different order of the preferred M in Figure 7, namely, (Pr, Ba) > W > (P, Ta) for a, while (P, Ta) > W > (Pr, Ba) for b, is mainly due to different amounts of desorbed oxygen between eqs 1 and 3 and is not due to the different structure (spinel or rocksalt).

Further, we discuss the effect of elemental substitution on the suppression of phase transformation. The transformation to rocksalt tends to be suppressed in high-valence elements. For the stability of the layered rocksalt, the effect on the e_g orbital, which is a hybrid orbital of Ni 3d and O 2p, can be important. In Li_xNiO_2, the e_g orbital changes from partially occupied to unoccupied as x decreases. This means that the contribution of the O 2p orbital in the valence band decreases, and O in the layered rocksalt becomes unstable because its contribution to O bonding is smaller.[36] In other words, high-valence elements are able to suppress O desorption because the e_g orbital can remain partially occupied. In terms of the stability of the rocksalt structure, to maintain the charge neutrality, O desorption becomes more difficult when high-valence elements are in solid solution. Therefore, it is inferred that the formation of the rocksalt structure is suppressed.

Transformation to the spinel structure tends to be suppressed by elements with large ionic radii, such as lanthanides and alkaline earth metals, rather than high-valence elements. The difference in effective elements from the rocksalt may be due to the fact that the valence of Ni is more variable in the spinel because of the smaller amount of oxygen desorption and the charge neutrality. Therefore, compared to the transformation to rocksalt, local distortion due to the difference in ionic radius with Ni is presumed to be more influential than chemical bonding.

4.3. M to Be Adopted to Suppress Pyrolysis. The practical interest eventually concerns the M to be adopted as the substituent to suppress pyrolysis. Adopting M = P and Ta, the prediction, Figure 7, indicates that the substituents promote a spontaneous transformation to spinel. The choice is obviously not desirable in terms of degradation of the cathode material. From this viewpoint, the choice M = Pr and Ba is predicted to be the best in suppressing the degradation as it provides the highest reaction enthalpy ΔH toward the initial transformation to spinel (see Figures 6 and 7). Adopting M = W, the suppression against the degradation continues to work with reduced ΔH, but the choice is superior in suppressing the subsequent reaction toward rocksalt (causing dangerous incidents, such as ignition) as compared to the choice M = Pr and Ba. Since the most important motivation of this study was the design to avoid the risk of ignition or explosion for high-capacity batteries, the choice of M = W would be of great importance. Again, the choice M = P and Ta shows the highest suppression against the dangerous transition to the rocksalt, but the spontaneous degradation toward the spinel structure nevertheless implies that the choice is not desirable.

With regard to this investigation, we determined that W is the key element to prevent thermal runaway. To this end, we discuss the effect of W on capacity. In the literature, where the effect on the charge−discharge profile was calculated from first-principles, the voltage drops due to the addition of W were comparable to that of Co.[11] This means that additional thermal stability can be expected at the same capacity as that with Co addition.

4.4. Further Development for the Prediction of Thermal Stability. In this study, we investigated the effect of element substitution on the thermal stability of cathode materials by using reaction enthalpies for modeling. In this

https://doi.org/10.1021/acsami.2c01607
ACS Appl. Mater. Interfaces 2022, 14, 23355−23363

section, we discuss the factors that are not fully taken into consideration, the effect of those approximations on the predicted results, and the prospects for further development of the model to simulate more complex cathode materials.

First, the ease of cation mixing and oxygen desorption during pyrolysis is not explicitly considered. These are expected to vary with the substituted elements. In the bulk, these can be interpreted as elementary processes of the reaction, and their combination is expected to define the reaction barrier. In contrast, the influence of substitution elements on the combined order of these two elementary processes must be carefully considered. Therefore, it is necessary to understand the mechanism of the effect of elemental substitution, both experimentally and theoretically.

For further development, surface and interface effects must also be considered. Since thermal decomposition is often the starting point for reactions at particle surfaces and interfaces, the thermal stability of cathode materials also depends on surface modifications and coatings. Screening the influence of solid-soluble elements on the reactivity of such surfaces requires calculations in unit cells with an order of magnitude of at least 100 atoms.

Differences in the solid solubility of added elements in LNO also merit further study. Some elements tend to segregate on surfaces and interfaces, which can greatly increase or decrease the effectiveness of pyrolysis suppression. In contrast, since cathode materials are generally synthesized under high temperatures (600−800 °C), it is important to consider their solid solubility at high temperatures as well. The development of technology to perform such thermodynamic calculations for unknown compositions in a simple manner will make it possible to design compositions that include solid solubility.

Li/Ni cation mixing during synthesis also requires further investigation. Cation mixing of Li/Ni or Li/M during synthesis may lead to more thermodynamically unstable or more stable initial structures. It is possible that elements will be discovered for which cation mixing is the primary controlling factor and for which the thermal stability can be significantly improved. On the other hand, if cation mixing during synthesis is to be considered, it is necessary to examine the Li/(Ni + M) ratio under various conditions to determine which composition is more stable. Although this is an interest for the future, a large number of combinations of compositions and cation mixing structures would be required. In addition, we should also consider that the introduction of cation mixing may reduce the amount of Li extracted, resulting in a significant decrease in battery capacity.

5. CONCLUSION

We considered a design of cathode materials for high-capacity LNO-based batteries that suppresses the pyrolysis reactions via atomic substitutions. Ab initio simulations were performed to investigate which substituent M realizes the higher enthalpy barrier against pyrolysis. To evaluate the barrier using the calculations, several reaction models were developed to describe the pyrolysis processes, and the enthalpies of formation were compared. The proposed candidate models were narrowed down based on trend matching with experimental data. We analyzed the correlation of the predictability with respect to the M-substitution effect among the remaining reaction models to identify the factors controlling the choice of reaction model and the predictability. As a result, we found that the difference in the amount of oxygen desorption in the models has a significant effect on the predictability of the M-substitution effect. The choice with M = P and Ta is predicted to achieve the highest enthalpy barrier in reaching the eventual phase of the pyrolysis with the cubic rocksalt structure, wherein large oxygen desorption leads to dangerous incidents such as ignition or explosion. These choices, however, are not appropriate from the point of view of degradation of the cathode material, as they promote the metamorphosis to the spinel structure as a degradation. M = Pr and Ba was predicted to be a good choice to prevent the degradation to the spinel structure but had a lower barrier to rocksalt than M = P and Ta. M = W achieves suppression against both the degradation toward the spinel structure as well as the eventual transition to rocksalt, though the barriers are slightly lower than the best value. The above observations on M = P and Ta indicate that it is important to consider not only the whole reaction barrier but also the initial reaction barrier to achieve a proper substitution to suppress pyrolysis.

■ ASSOCIATED CONTENT

Supporting Information

The Supporting Information is available free of charge at https://pubs.acs.org/doi/10.1021/acsami.2c01607.

Full details of differential scanning calorimetry (DSC) experiments and ab initio calculations (PDF)

■ AUTHOR INFORMATION

Corresponding Author

Yuki Yoshimoto − *Department of Computer-Aided Engineering and Development, Sumitomo Metal Mining Co., Ltd., Niihama, Ehime 792-0001, Japan;* orcid.org/0000-0002-8027-3118; Email: yuki.yoshimoto.d2@smm-g.com

Authors

Takahiro Toma − *Battery Research Laboratories, Sumitomo Metal Mining Co., Ltd., Niihama, Ehime 792-0002, Japan;* orcid.org/0000-0001-8698-9742

Kenta Hongo − *Research Center for Advanced Computing Infrastructure, JAIST, Nomi, Ishikawa 923-1292, Japan;* orcid.org/0000-0002-2580-0907

Kousuke Nakano − *School of Information Science, JAIST, Nomi, Ishikawa 923-1292, Japan;* orcid.org/0000-0001-7756-4355

Ryo Maezono − *School of Information Science, JAIST, Nomi, Ishikawa 923-1292, Japan;* orcid.org/0000-0002-5875-971X

Complete contact information is available at: https://pubs.acs.org/10.1021/acsami.2c01607

Notes

The authors declare no competing financial interest.

■ ACKNOWLEDGMENTS

This work used computational resources of Fujitsu PRIMERGY CX2550/CX2560 M4 (ITO Subsystem A) provided by Research Institute for Information Technology at Kyushu University through the HPCI System Research Project (Project ID: hp200054), Fujitsu PRIMERGY CX400M1/CX2550M5 (Oakbridge-CX) provided by Information Technology Center at The University of Tokyo through the HPCI System Research Project (Project ID: hp210055), and the PC Cluster System provided by the facilities of Research Center

for Advanced Computing Infrastructure at the Japan Advanced Institute of Science and Technology (JAIST). Y.Y. would like to thank T. Yoshida and S. Yoshio for fruitful discussions and technical support. K.H. is grateful for financial support from MEXT-KAKENHI (JP16H06439, JP19K05029, JP19H05169, and JP21K03400) and the Air Force Office of Scientific Research (Award FA2386-20-1-4036). R.M. is grateful for the financial support from MEXT-KAKENHI (JP21K03400 and JP19H04692), the Air Force Office of Scientific Research (AFOSR-AOARD/FA2386-17-1-4049; FA2386-19-1-4015), and JSPS Bilateral Joint Projects (JPJSBP120197714).

REFERENCES

(1) Xu, J.; Lin, F.; Doeff, M. M.; Tong, W. A review of Ni-based layered oxides for rechargeable Li-ion batteries. *J. Mater. Chem. A* **2017**, *5* (3), 874−901.

(2) Schipper, F.; Erickson, E. M.; Erk, C.; Shin, J.-Y.; Chesneau, F. F.; Aurbach, D. Review—Recent Advances and Remaining Challenges for Lithium Ion Battery Cathodes. *J. Electrochem. Soc.* **2017**, *164* (1), A6220.

(3) Liu, W.; Oh, P.; Liu, X.; Lee, M. J.; Cho, W.; Chae, S.; Kim, Y.; Cho, J. Nickel-Rich Layered Lithium Transition-Metal Oxide for High-Energy Lithium-Ion Batteries. *Angew. Chem., Int. Ed.* **2015**, *54* (15), 4440−4457.

(4) de Biasi, L.; Kondrakov, A. O.; Geßwein, H.; Brezesinski, T.; Hartmann, P.; Janek, J. Between Scylla and Charybdis: Balancing among Structural Stability and Energy Density of Layered NCM Cathode Materials for Advanced Lithium-Ion Batteries. *J. Phys. Chem. C* **2017**, *121* (47), 26163−26171.

(5) Sun, Y. K.; Myung, S. T.; Park, B. C.; Prakash, J.; Belharouak, I.; Amine, K. High-energy cathode material for long-life and safe lithium batteries. *Nat. Mater.* **2009**, *8* (4), 320−324.

(6) Li, W.; Song, B.; Manthiram, A. High-voltage positive electrode materials for lithium-ion batteries. *Chem. Soc. Rev.* **2017**, *46* (10), 3006−3059.

(7) Bianchini, M.; Roca-Ayats, M.; Hartmann, P.; Brezesinski, T.; Janek, J. There and Back Again-The Journey of $LiNiO_2$ as a Cathode Active Material. *Angew. Chem., Int. Ed.* **2019**, *58* (31), 10434−10458.

(8) Yoshida, T.; Maezono, R.; Hongo, K. Synergy of Binary Substitution for Improving Cycle Performance in $LiNiO_2$ Revealed by ab Initio Materials Informatics. *ACS Omega* **2020**, *5* (22), 13403−13408.

(9) Yoshida, T.; Hongo, K.; Maezono, R. First-Principles Study of Structural Transition in $LiNiO_2$ and High Throughput Screening for Long Life Battery. *J. Phys. Chem. C* **2019**, *123* (23), 14126−14131.

(10) Toma, T.; Maezono, R.; Hongo, K. Electrochemical Properties and Crystal Structure of Li^+/H^+ Cation-exchanged $LiNiO_2$. *ACS Appl. Energy Mater.* **2020**, *3* (4), 4078−4087.

(11) Yoshio, S.; Hongo, K.; Nakano, K.; Maezono, R. High-throughput evaluation of discharge profiles in $LiNi_{1-x}X_xO_2$ by ab initio calculations. *J. Phys. Chem. C* **2021**, *125* (27), 14517−14524.

(12) Zhang, Z.; Fouchard, D.; Rea, J. R. Differential scanning calorimetry material studies: implications for the safety of lithium-ion cells. *J. Power Sources* **1998**, *70* (1), 16−20.

(13) Belharouak, I.; Lu, W.; Vissers, D.; Amine, K. Safety characteristics of $Li(Ni_{0.8}Co_{0.15}Al_{0.05})O_2$ and $Li(Ni_{1/3}Co_{1/3}Mn_{1/3})O_2$. *Electrochem. Commun.* **2006**, *8* (2), 329−335.

(14) Dahn, J. R.; Fuller, E. W.; Obrovac, M.; von Sacken, U. Thermal stability of Li_xCoO_2, Li_xNiO_2 and -MnO_2 and consequences for the safety of Li-ion cells. *Solid State Ion* **1994**, *69* (34), 265−270.

(15) Yoon, W. S.; Chung, K. Y.; McBreen, J.; Yang, X. Q. A comparative study on structural changes of $LiCo_{1/3}Ni_{1/3}Mn_{1/3}O_2$ and $LiNi_{0.8}Co_{0.15}Al_{0.05}O_2$ during first charge using in situ XRD. *Electrochem. Commun.* **2006**, *8* (8), 1257−1262.

(16) Guilmard, M.; Croguennec, L.; Delmas, C. Thermal Stability of Lithium Nickel Oxide Derivatives. Part II: $Li_xNi_{0.70}Co_{0.15}Al_{0.15}O_2$ and $Li_xNi_{0.90}Mn_{0.10}O_2$ (x = 0.50 and 0.30). Comparison with $Li_xNi_{1.02}O_2$ and $Li_xNi_{0.89}Al_{0.16}O_2$. *Chem. Mater.* **2003**, *15* (23), 4484−4493.

(17) Guilmard, M.; Croguennec, L.; Denux, D.; Delmas, C. Thermal Stability of Lithium Nickel Oxide Derivatives. Part I: $Li_xNi_{1.02}O_2$ and $Li_xNi_{0.89}Al_{0.16}O_2$ (x = 0.50 and 0.30). *Chem. Mater.* **2003**, *15* (23), 4476−4483.

(18) Bak, S. M.; Nam, K. W.; Chang, W.; Yu, X.; Hu, E.; Hwang, S.; Stach, E. A.; Kim, K. B.; Chung, K. Y.; Yang, X. Q. Correlating Structural Changes and Gas Evolution during the Thermal Decomposition of Charged $Li_xNi_{0.8}Co_{0.15}Al_{0.05}O_2$ Cathode Materials. *Chem. Mater.* **2013**, *25* (3), 337−351.

(19) Bak, S. M.; Hu, E.; Zhou, Y.; Yu, X.; Senanayake, S. D.; Cho, S. J.; Kim, K. B.; Chung, K. Y.; Yang, X. Q.; Nam, K. W. Structural Changes and Thermal Stability of Charged $LiNi_xMn_yCo_zO_2$ Cathode Materials Studied by Combined In Situ Time-Resolved XRD and Mass Spectroscopy. *ACS Appl. Mater. Interfaces* **2014**, *6* (24), 22594−22601.

(20) Park, K.-J.; Jung, H.-G.; Kuo, L.-Y.; Kaghazchi, P. C.; Yoon, S.; Sun, Y.-K. Improved Cycling Stability of $Li[Ni_{0.90}Co_{0.05}Mn_{0.05}]O_2$ Through Microstructure Modification by Boron Doping for Li-Ion Batteries. Adv. *Energy Mater.* **2018**, *8* (25), 1801202.

(21) Xie, H.; Du, K.; Hu, G.; Peng, Z.; Cao, Y. The Role of Sodium in $LiNi_{0.8}Co_{0.15}Al_{0.05}O_2$ Cathode Material and Its Electrochemical Behaviors. *J. Phys. Chem. C* **2016**, *120* (6), 3235−3241.

(22) Pouillerie, C.; Croguennec, L.; Biensan, P.; Willmann, P.; Delmas, C. Synthesis and Characterization of New $LiNi_{1-y}Mg_yO_2$ Positive Electrode Materials for Lithium-Ion Batteries. *J. Electrochem. Soc.* **2000**, *147* (6), 2061−2069.

(23) Ohzuku, T.; Ueda, A.; Kouguchi, M. Synthesis and Characterization of $LiAl_{1/4}Ni_{3/4}O_2$(R-3m) for Lithium-Ion (Shuttlecock) Batteries. *J. Electrochem. Soc.* **1995**, *142* (12), 4033−4039.

(24) Yang, Z.; Guo, X.; Xiang, W.; Hua, W.; Zhang, J.; He, F.; Wang, K.; Xiao, Y.; Zhong, B. K-doped layered $LiNi_{0.5}Co_{0.2}Mn_{0.3}O_2$ cathode material: Towards the superior rate capability and cycling performance. *J. Alloys Compd.* **2017**, *699*, 358−365.

(25) Du, R.; Bi, Y.; Yang, W.; Peng, Z.; Liu, M.; Liu, Y.; Wu, B.; Yang, B.; Ding, F.; Wang, D. Improved cyclic stability of $LiNi_{0.8}Co_{0.1}Mn_{0.1}O_2$ via Ti substitution with a cut-off potential of 4.5V. *Ceram. Int.* **2015**, *41* (5), 7133−7139.

(26) Nishida, Y.; Nakane, K.; Satoh, T. Synthesis and properties of gallium-doped $LiNiO_2$ as the cathode material for lithium secondary batteries. *J. Power Sources* **1997**, *68* (2), 561−564.

(27) Zhang, Z.; Chen, D.; Chang, C. Improved electrochemical performance of $LiNi_{0.8}Co_{0.1}Mn_{0.1}O_2$ cathode materials via incorporation of rubidium cations into the original Li sites. *RSC Adv.* **2017**, *7* (81), 51721−51728.

(28) Zhang, M.; Zhao, H.; Tan, M.; Liu, J.; Hu, Y.; Liu, S.; Shu, X.; Li, H.; Ran, Q.; Cai, J.; Liu, X. Yttrium modified Ni-rich $LiNi_{0.8}Co_{0.1}Mn_{0.1}O_2$ with enhanced electrochemical performance as high energy density cathode material at 4.5 V high voltage. *J. Alloys Compd.* **2019**, *774*, 82−92.

(29) Wang, D.; Li, X.; Wang, Z.; Guo, H.; Xu, Y.; Fan, Y.; Ru, J. Role of zirconium dopant on the structure and high voltage electrochemical performances of $LiNi_{0.5}Co_{0.2}Mn_{0.3}O_2$ cathode materials for lithium ion batteries. *Electrochim. Acta* **2016**, *188*, 48−56.

(30) Steiner, J. D.; Cheng, H.; Walsh, J.; Zhang, Y.; Zydlewski, B.; Mu, L.; Xu, Z.; Rahman, M. M.; Sun, H.; Michel, F. M.; Sun, C.-J.; Nordlund, D.; Luo, W.; Zheng, J.-C.; Xin, H. L.; Lin, F. Targeted Surface Doping with Reversible Local Environment Improves Oxygen Stability at the Electrochemical Interfaces of Nickel-Rich Cathode Materials. *ACS Appl. Mater. Interfaces* **2019**, *11* (41), 37885−37891.

(31) Kim, Y. Effects and distribution of Zr introduced in Ni-based cathode material for Li-ion batteries. *Phys. Chem. Chem. Phys.* **2019**, *21* (23), 12505−12517.

(32) Cui, P.; Jia, Z.; Li, L.; He, T. Preparation and characteristics of Sb-doped $LiNiO_2$ cathode materials for Li-ion batteries. *J. Phys. Chem. Solids* **2011**, *72* (7), 899−903.

(33) Kim, U. H.; Jun, D. W.; Park, K. J.; Zhang, Q.; Kaghazchi, P.; Aurbach, D.; Major, D. T.; Goobes, G.; Dixit, M.; Leifer, N.; Wang, C. M.; Yan, P.; Ahn, D.; Kim, K. H.; Yoon, C. S.; Sun, Y. K. Pushing the limit of layered transition metal oxide cathodes for high-energy

https://doi.org/10.1021/acsami.2c01607
ACS Appl. Mater. Interfaces 2022, 14, 23355−23363

density rechargeable Li ion batteries. *Energy Environ. Sci.* **2018**, *11* (5), 1271−1279.
(34) Wang, L.; Maxisch, T.; Ceder, G. A First-Principles Approach to Studying the Thermal Stability of Oxide Cathode Materials. *Chem. Mater.* **2007**, *19* (3), 543−552.
(35) Momma, K.; Izumi, F. VESTA 3 for three-dimensional visualization of crystal, volumetric and morphology data. *J. Appl. Crystallogr.* **2011**, *44*, 1272−1276.
(36) Laubach, S.; Laubach, S.; Schmidt, P. C.; Ensling, D.; Schmid, S.; Jaegermann, W.; Thißen, A.; Nikolowski, K.; Ehrenberg, H. Changes in the crystal and electronic structure of LiCoO2 and LiNiO2 upon Li intercalation and de intercalation. *Phys. Chem. Chem. Phys.* **2009**, *11*, 3278−3289.

https://doi.org/10.1021/acsami.2c01607
ACS Appl. Mater. Interfaces 2022, 14, 23355−23363